Multi-scale segmentation of dual-channel MRI using volume resolution enhancement and tubular structure detection

James Withers[a]*, Mark Bastin[b] and Amos Storkey[c]

[a]Neuroinformatics Doctoral Training Centre, University of Edinburgh, [b]Medical Physics, University of Edinburgh, [c]Institute for Adaptive and Neural Computation, University of Edinburgh

Abstract. Brain tissue segmentation is complicated by noise and partial volume voxels that contain mixtures of two or more tissue types. We examine three extensions to segmentation methods which may allow more accurate classification of small-scale structures while still providing robustness to noise. Firstly, the location and orientation of fine tubular structures can be identified using differential geometry. Subsequent neighbourhood filtering operations, for ensuring local homogeneity or performing resolution enhancement of the volume, may then operate with different scales and orientations according to the structure of interest. Finally, dual-channel T2-PD segmentation can be improved by weighting the information from each modality to better emphasise contrasting tissues. We present quantitative results on simulated volumes and qualitative assessments on a real dataset, discuss limitations and improvements to the methods, and examine future application to an Expectation-Maximisation framework.

1 Introduction

The automatic segmentation of brain volumes – usually into gray matter, white matter, cerebrospinal fluid (CSF) and blood/background – is necessary for analyses based on tissue type and volume quantification. MRI is able to produce a range of tissue contrasts, but in clinical practice confounds to successful segmentation include various sources of noise, low resolution, ambiguous partial volumes (where multiple tissues reside in a single voxel), and poor contrast between some tissues in certain modalities. Many approaches to limiting the effects of noise enforce local class or intensity homogeneity (i.e. [1]). An unfortunate consequence of processing neighbourhood interactions at a single scale is that small details can be smoothed over like the noise. In particular, Diffusion Tensor Imaging can benefit from accurate and detailed tissue maps in order to provide robust procession and termination criteria for tractography methods.

In this paper we present several extensions to previously-developed methods that aid segmentation; primarily, we incorporate multi-scale oriented filters for protecting thin structures while still providing robustness to noise, introduced by Svensson *et al*. [2]. Brain atlases (as used in [3]) are formed from averages over a population and thus cannot provide strong priors for the precise layouts of cortical sulci and blood vessels which are unique between brains. Sato *et al*. [4] have investigated using differential geometry in general multi-channel segmentation, and Descoteaux *et al*. [5] have used similar filters to detect the centrelines of blood vessels. This approach is generally fast and robust, but morphological methods (such as [6]) have also been used to detect such structures. The majority of segmentation approaches deal with T1-weighted volumes due to their excellent gray and white matter contrast, but the best modalities for detecting cortical sulci and blood vessels were found to be T2 and proton density (PD) respectively. Consequently steps are taken to exploit multi-channel data in segmentation, as investigated by Liang *et al*. [7]. Finally, in order to process small structures at more relevant scales, volume upsizing with partial volume reduction [8] is employed. A further anisotropic smoothing step [9], first investigated in brain MRI by Gerig *et al*. [10], aims to reduce noise while also preserving detail.

2 Methods

The implementation of Fuzzy C-Means (FCM) clustering by Ahmed *et al*. [11] was chosen to demonstrate the following improvements. Given intensities X (indexed by voxels i) and centroids V for C classes, the objective function J weights the information gained from a central voxel with that from its $3 \times 3 \times 3$ neighbourhood N using parameter α:

$$J = \sum_{i \in volume} \sum_{k=1}^{C} u_{ik}^{p} \left\| x_i - v_k \right\|^2 + \frac{\alpha}{\text{numel}(N)} \sum_{i \in image} \sum_{m=1}^{C} u_{im}^{p} \sum_{j \in N_i} \left\| x_j - v_m \right\|^2 \quad (1)$$

In noisy images α should be increased to produce a more homogeneous result. u defines the tissue class memberships at each voxel, and p is a positive exponent controlling the fuzziness of the segmentation result. The algorithm is fast and robust, but tends to erode small details due to the drive for homogeneity using a single neighbourhood filter, and it can perform poorly when contrast is low – such as between background/blood and CSF in T1-weighted volumes.

*E-mail: s0456265@sms.ed.ac.uk

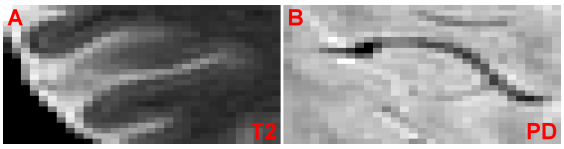

Figure 1. Thin structures in brain volumes. (**A**) Cortical sulci (bright in T2) can possess complex topology, often flaring near the brain surface. (**B**) Blood vessels (dark in PD) are tubular structures that form smooth arcs and junctions.

2.1 Thin structure detection using differential geometry

Tubular structures possess a direction of minimal intensity curvature which coincides with the orientation of the tube, and an orthogonal direction (or plane in 3D) of maximal curvature where intensity reaches a local extremum at the medial axis. Blood vessels are naturally tubular but thin cortical sulci also appear as such in 2D (Fig 1). Sulci are CSF-filled fissures with a tightly-packed and complex 3D structure caused by the folding of the cortex, making 3D filters that may respond optimally to plate-like shapes slightly less accurate than their 2D counterparts at the appropriate orientation. The proposed filter for locating both the presence and orientation of tubular structures is based on eigenvalue analysis of the Hessian [12]: the eigenvector associated with the smallest eigenvalue λ_2 represents the direction of minimal curvature, and the eigenvector of λ_1 gives the direction of maximal curvature. The sign of λ_1 discriminates between local intensity minima and maxima, so MRI modalities can be chosen that best contrast the structures of interest: CSF is much brighter than other tissues in T2-weighted volumes, and blood is very dark in PD volumes.

Frangi *et al*. [12] introduce R_B, which assesses adherence to an optimal tube profile ($\lambda_1 \gg \lambda_2$), and S, the Euclidean norm of the eigenvalues, which is small for noise and highest in blob-like areas, which include structures proceeding in the through-plane direction and junctions. A parameter s refers to the scale space level for the Hessian, which allows structures of different sizes to be optimally detected. The tubular structure filter T (Eqns 2 and 3) took the maximum response over a range of scales, but because tissue contrasts are dependent on the scan sequences used, a threshold was set to achieve a $\sim$99% positive predictive value on labelled data for voxels containing the mapped tissue.

$$T_{sulci}(s) = \begin{cases} 0, & \text{if } \lambda_1 \geq 0; \\ (1 - e^{-S}) * e^{-R_B}, & \text{if } \lambda_1 < 0. \end{cases} \quad (2) \qquad T_{blood}(s) = \begin{cases} 0, & \text{if } \lambda_1 \leq 0; \\ (1 - e^{-S}) * e^{-R_B}, & \text{if } \lambda_1 > 0. \end{cases} \quad (3)$$

2.2 Volume resolution enhancement to reduce the relative amount of partial volume voxels

Salvado *et al*. [8] developed an interpolation scheme where intensity could diffuse between subvoxels on an upsized volume to reduce the relative amount of partial volume on tissue boundaries. This process, along with a further anisotropic smoothing step [9], will be referred to as *volume resolution enhancement*. Gaussian smoothing reduces both noise and the intensity extrema of thin structures when calculating the diffusion gradients, but the pre-computed minimum curvature direction is able to bias the filtering: a smaller, tighter, ellipsoid 3D Gaussian oriented in parallel to the structure can better preserve the intensity (Fig 2). Also, less diffusion occurs than expected around thin contrasting structures since local rank ordering limits (which dictate the amount of possible flow) can sometimes overlook their extreme intensties. The limits are set further from the median in these regions.

2.3 Modifications to Fuzzy C-Means clustering

Multi-scale oriented filters can also be applied to neighbourhood schemes for segmentation that aim to homogenise the local class or intensity. In our exemplar segmentation method (Eqn 1), the intensities of 26 neighbours are considered of equal importance. A larger neighbourhood can be considered for improved noise reduction by employing a normalised Gaussian filter G to weight the local information by the distance from the central voxel (*dist*) in a similar fashion to

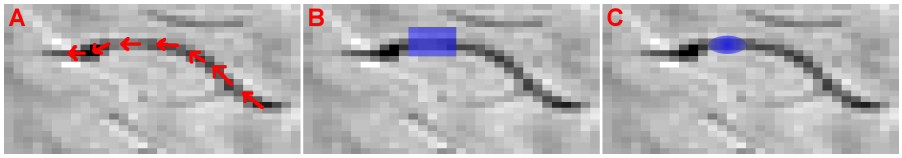

Figure 2. Multi-scale oriented filters help to preserve thin structures. (**A**) The direction of minimal curvature (red arrows) can be mapped using differential geometry. (**B**) Thin structures are blurred due to their small size compared to the isotropic filter dimensions (blue box). (**C**) By tailoring the filter size, profile and orientation (radial blue ellipse), the valid neighbourhood is altered and the structures can be better preserved.

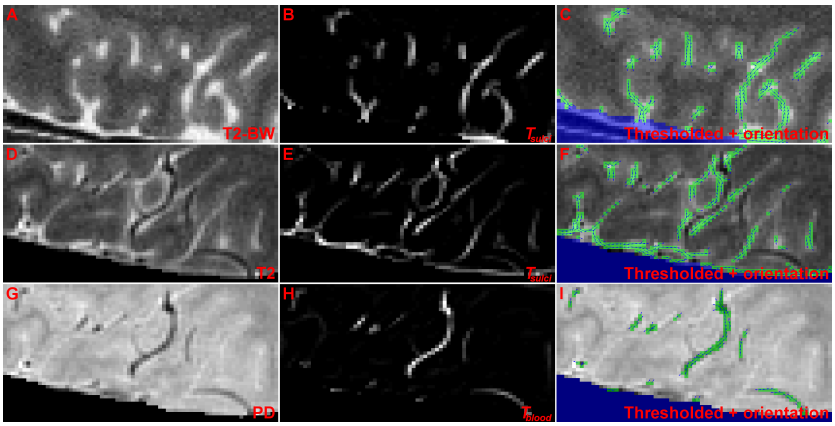

Figure 3. Detection of thin structures. (**A**-**C**) Detection of cortical sulci in temporal cortex of a BrainWeb T2-weighted volume. (**D**-**F**) Detection of sulci in temporal cortex of a real T2-weighted volume. (**G**-**I**) Detection of blood vessels in temporal cortex of a real PD volume. **Left**: volume intensities. **Middle**: Continuous map of T. **Right**: Thresholded T in green, non-brain voxels in blue, and direction of minimal curvature denoted with small blue arrows.

Shen *et al*. [13]. Thin tubular structures can be protected by orienting the filters and reducing their profile σ in these areas. The updated form of Eqn 1 uses resolution-enhanced T2-weighted and PD volumes $\bar{X}$ indexed by subvoxels z:

$$J_{modified} = \sum_{z \in volume} \sum_{k=1}^{C} u_{zk}^{p} \left\| w_k(\bar{x}_z - v_k) \right\|^2 + \alpha \sum_{z \in volume} \sum_{m=1}^{C} u_{zm}^{p} \sum_{j \in N_z} G(dist(z,j), \sigma_z) \left\| w_m(\bar{x}_j - v_m) \right\|^2 \quad (4)$$

The weight matrix W exploits the quality of modality-specific tissue class contrasts: it enforces that well-contrasting tissue in one modality is more sensitive to deviation from its centroid than poorly contrasting tissue. The tuning of W could be approached by searching to maximise performance over a labeled dataset, but the values were set intuitively in the following tests. T2 has a greater weight for its bright CSF but less for white matter, which is poorly separated from the remaining classes. PD has an increased weight for the well-contrasted white matter, but reduced for CSF, which can be difficult to distinguish from gray matter. The other weights were set to unity.

3 Results

5 central axial slices of synthetic brain volumes generated by BrainWeb [14] with 3% added noise were used for quantitative evaluation. The ground truth is already known since the volumes are constructed from a set of constituent class maps. Real T2-weighted and PD MRI volumes were acquired using a dual-echo Fast Spin Echo sequence on a 1.5T scanner at the Western General Hospital, Edinburgh, UK. The voxels were isotropic and other scan parameters were $NEX = 1$, TE_{PD} = 15ms, TE_{T2} = 100ms, FOV = 240mm and matrix size 256×256. As a preprocessing step the brain was extracted from the volume and BFC [15] was used to correct for the bias field.

3.1 Tubular structure detection accuracy

BrainWeb volumes do not contain blood vessels, and so quantitative evaluation was performed on cortical sulci only using $s \in [0.5...0.85]$, corresponding to the expected range of the shorter dimension of the structures. The evaluation criterion was the correct presence of any CSF in voxels flagged by a threshold on T_{sulci}; since the threshold was set to ensure a $\sim$99% positive predictive value, the other error statistics are more informative (Table 1). The frequency of false positives doubles at the 5% BrainWeb volume noise level using the same threshold, but this error rate is still extremely small. Furthermore, since the small structure maps are not being used as tissue class priors but instead only as detail filter selectors, errors will only manifest as increasing the influence from immediate (perhaps noisy) neighbours and ideally have minimal impact on the segmentation result. Only half of the voxels containing CSF are detected, but a significant proportion of the remainder are found in larger blob-like structures such as the ventricles. These areas do not display a thin profile and therefore should not be detected. Fig 3 shows the performance of T_{sulci} in real and simulated images, and T_{blood} in real images only. The same threshold was applied to both rounds of sulcal detection. Blob-like structures tend to scatter the directions of minimal curvature, as would be expected, whereas their continuity along thin sulci and blood vessels is generally excellent.

	Ground truth		
	CSF present	**No CSF present**	
Thresholded	12209 (TP)	192 (FP)	**PPV:** 98.45%
Not thresholded	12613 (FN)	75076 (TN)	**NPV:** 85.62%
	Sensitivity: 49.19%	**Specificity:** 99.74%	

Table 1. Error statistics of CSF voxels flagged by thin structure detection against the BrainWeb ground truth. 100090 voxels were examined in total. TP = true positive. FP = false positive. TN = true negative. FN = false negative. PPV = positive predictive value. NPV = negative predictive value.

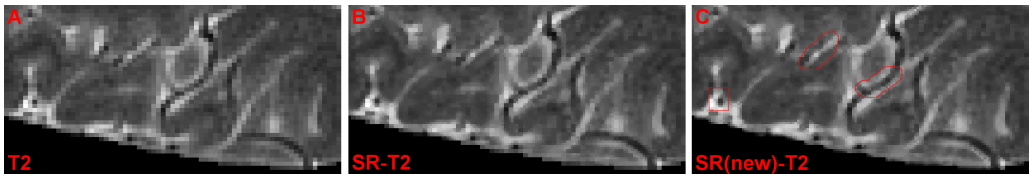

Figure 4. Improved crispness of resolution-enhanced thin structures. (**A**) Temporal cortex in a real T2-weighted volume. (**B**) Original $2 \times 2 \times 2$ resolution-enhanced version of (A). (**C**) Improved resolution enhancement of (A).

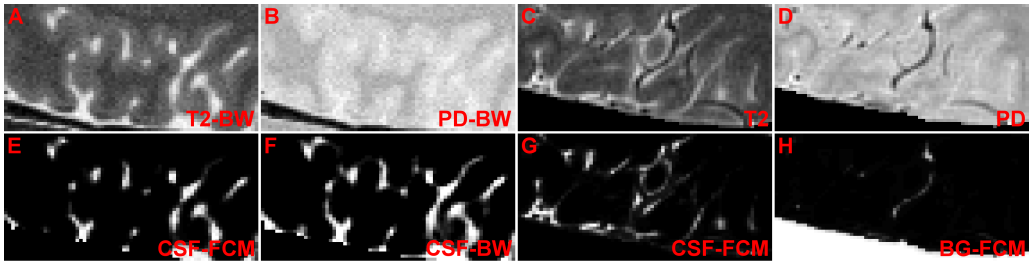

Figure 5. Segmentation accuracy. (**A** & **B**) Temporal cortex in BrainWeb T2-weighted and PD volumes. (**C** & **D**) Similar area in real volumes. (**E**) CSF memberships from (A) and (B) using modified FCM. (**F**) Ground truth CSF proportions. (**G** & **H**) CSF and blood/background memberships from (C) and (D) using modified FCM.

3.2 Changes in volume resolution enhancement quality

The results in Figs 4 and 5 and Table 2 were produced over 30 iterations with the diffusion speed $dt = 0.2$, using a $2 \times 2 \times 2$ resizing ratio. Resolution enhancement of a real T2-weighted image of temporal cortex is shown in Fig 4; the ringed areas show particular areas of improvement, in terms of the crispness of tissue borders.

3.3 Improvements in overall segmentation quality

The class centroids were initialised uniformly in the intensity space and clustering continued until the sum of their changes was less than 0.01. The modified process (Eqn 4) consistently outperformed the original (Eqn 1) in segmenting dual-channel data (Table 2). Since FCM produces class memberships, rather than physical proportions of mixtures, the difference between the output and the ground truth is displayed purely for comparative purposes. In real brain volumes the partial volume effects caused by the thinness of blood vessels mean they appear closest in intensity to other classes. As FCM is not able to intelligently disambiguate mixtures, the vessels in Fig 5H are mostly labelled as white matter, with darker regions gaining some contribution from blood, despite their excellent detection (Fig 3H).

4 Discussion

Our applications of eigenvalue analysis include increasing allowed flow during volume resolution enhancement processes, using the minimum curvature direction to change neighbourhood filter orientations, and tightening filter profiles in thresholded areas, in order to encourage the preservation of thin structures such as cortical sulci and blood vessels. We have presented a unified and simple model for detecting these structures which can achieve a good sensitivity while maintaining excellent specificity. T2-weighted and PD volumes produce the best contrast for these structures and by introducing a weighting vector to compensate for the individual modalities' poor contrasts and to exploit exceptional ones, then this dual-channel data is able to discriminate well between all four tissue types. T1-weighted volumes typically have poor contrast between CSF and background/blood, both appearing dark. T2-weighted and PD volumes can be acquired with a dual-echo sequence, without adding registration artefacts, enabling dual-channel segmentation.

The most costly parameter is the upsizing ratio for volume resolution enhancement: greater reduction in partial volume at tissue borders comes at the cost of increased the time and memory requirements, so practical concerns limit this ratio

	BrainWeb	**Original FCM**		**Modified FCM**	
	# voxels	Diff ($\pm\sigma$)	✓label	Diff ($\pm\sigma$)	✓label
WM	48732	0.12 ± 0.09	77.98%	0.11 ± 0.09	78.63%
GM	65230	0.13 ± 0.11	64.20%	0.10 ± 0.09	67.29%
CSF	25947	0.04 ± 0.06	49.56%	0.03 ± 0.08	51.87%
All	100090	0.30 ± 0.21	93.57%	0.26 ± 0.21	94.67%

Table 2. Evaluation of FCM clustering changes. *Diff*: mean difference between class memberships u and BrainWeb ground truth. ✓*label*: frequency of matching the maximum classes in u and ground truth. *# voxels*: number of voxels containing any of this tissue. WM = white matter. GM = gray matter.

to $3 \times 3 \times 3$. The regular and detail filter profiles (the standard deviation in each axis) were both proportional to this ratio. Large changes to the rank order limits cause adverse effects on the robustness of the resolution enhancement, so the change in detail areas was kept small. If the distribution of the widths of sulci or vessels change, due to age-related effects or altering the imaging resolution, a different range of Hessian analysis scales may be necessary.

Most sulci in the BrainWeb slices studied proceeded through the axial plane and only this 2D plane was considered in the production of T; by selecting the maximum response over several planes (i.e. sagittal and coronal) the sensitivity should improve and the minimal curvature vector should be more realistic. Alternatively, further investigation of 3D structure measures discussed by Frangi *et al.* [12] may prove fruitful, and the detection sensitivity of blood vessels – often badly affected by partial volume – is expected to increase with 3D processing due to their cylindical profile. Furthermore, their maps could benefit from diffusion processes aiming to reduce noise along the vessels' lengths [16]. We have shown the intensity curvature to extrema that gives the optimum responses to T is applicable in real volumes but the resulting orientation field could be made more robust by using a filtering step [17]. In order to further tailor the structure preservation process the filter profiles could be changed proportionally to the optimal scale for each voxel.

FCM has been shown to perform poorly in the disambiguation of tissue mixtures; the proposed application of this work is to improve more advanced tools. *FAST* [1] uses a Markov random field prior to influence the labeling of voxels, that could benefit from employing multi-scale oriented filters to preserve thin details. *Segment* [3] uses prior class maps but only weak priors can exist for the uniquely-positioned blood vessels and cortical sulci. T_{sulci} and T_{blood} could provide stronger priors to help disambiguate the mixture components, if they maintain high positive predictive values.

Acknowledgements

This work is funded by the Engineering and Physical Sciences Research Council and the Medical Research Council. We are grateful to Olivier Salvado for supplying the volume resolution enhancement code.

References

1. Y. Zhang, M. Brady & S. Smith. "Segmentation of brain MR images through a hidden Markov random field model and the expectation-maximization algorithm." *IEEE Transactions on Medical Imaging* **20(1)**, pp. 45–57, 2001.
2. B. Svensson, M. Andersson, O. Smedby et al. "Efficient 3-D adaptive filtering for medical image enhancement." In *Proceedings of the IEEE International Symposium on Biomedical Imaging*, pp. 996–999. 2006.
3. J. Ashburner & K. Friston. "Unified segmentation." *Neuroimage* **26(3)**, pp. 839–851, 2005.
4. Y. Sato, C.-F. Westin, A. Bhalerao et al. "Tissue classification based on 3D local intensity structures for volume rendering." *IEEE Transactions on Visualization and Computer Graphics* **6(2)**, pp. 160–180, 2000.
5. M. Descoteaux, D. Collins & K. Siddiqi. "Geometric flows for segmenting vasculature in MRI: theory and validation." In *Proceedings of Medical Image Computing and Computer-Assisted Intervention*, pp. 500–507. 2004.
6. L. Lorigo, O. Faugeras, W. Grimson et al. "CURVES: Curve evolution for vessel segmentation." *Medical Image Analysis* **5**, pp. 195–206, 2001.
7. Z. Liang, J. MacFall & D. Harrington. "Parameter estimation and tissue segmentation from multispectral MR images." *IEEE Transactions on Medical Imaging* **13(3)**, pp. 441–449, 1994.
8. O. Salvado, C. Hillenbrand & D. Wilson. "Partial volume reduction by interpolation with reverse diffusion." *International Journal of Biomedical Imaging* **1**, pp. 1–13, 2006.
9. O. Salvado & D. Wilson. "Thick slice interpolation using reverse anisotropic diffusion to reduce partial volume effect." In *Proceedings of IEEE International Symposium on Biomedical Imaging: Nano to Macro*, pp. 1000–1003. 2006.
10. G. Gerig, O. Kubler, R. Kikinis et al. "Nonlinear anisotropic filtering of MRI data." *IEEE Transactions on Medical Imaging* **1(2)**, pp. 221–232, 1992.
11. M. Ahmed, S. Yamany, N. Mohamed et al. "A modified fuzzy C-means algorithm for bias field estimation and segmentation of MRI data." *IEEE Transactions on Medical Imaging* **21(3)**, pp. 193–199, 2002.
12. A. Frangi, W. Niessen, K. Vincken et al. "Multiscale vessel enhancement filtering." In *Proceedings of Medical Image Computing and Computer-Assisted Intervention*, pp. 130–137. 1998.
13. S. Shen, W. Sandham, M. Granat et al. "MRI fuzzy segmentation of brain tissue using neighbourhood attraction with neural network optimization." *IEEE Transactions on Information Technology in Biomedicine* **9(3)**, pp. 459–467, 2005.
14. C. Cocosco, V. Kollokian, R.-S. Kwan et al. "Brainweb: online interface to a 3D MRI simulated brain database." *NeuroImage* **5(4)**, pp. S425, 1997.
15. D. Shattuck, S. Sandor-Leahy, K. Schaper et al. "Magnetic resonance image tissue classification using a partial volume model." *Neuroimage* **13**, pp. 856–876, 2001.
16. R. Manniesing, M. Viergever & W. Niessen. "Vessel enhancing diffusion A scale space representation of vessel structures." *Medical Image Analysis* **10(6)**, pp. 815–825, 2006.
17. C.-F. Westin & H. Knutsson. "Tensor field regularization using normalized convolution." In *Proceedings of the International Conference on Computer Aided Systems Theory*, pp. 564–572. 2003.